On the mechanics of chip formation in Ti6Al4V turning with spindle speed variation

Elio Chiappini[1], Stefano Tirelli[1], Paolo Albertelli[2], Matteo Strano[2], Michele Monno[2]
[1]Laboratorio MUSP, via Tirotti 9, 29122 Piacenza (Italy)
[2]Mechanical Engineering Department, Politecnico di Milano, via La Masa 1, 20156 Milano (Italy)

Abstract

Titanium alloys are hard-to-cut materials and need to be machined at relatively low cutting speeds with obvious negative consequences on the profitability of machining.
In order to enhance material removal rate (MRR), a strategy that relies on higher depths of cut could be chosen if vibrational issues due to regenerative chatter did not occur.
A lot of research was done to suppress regenerative chatter without detrimental effects on productivity. One of the most interesting chatter suppression methods, mainly due to its flexibility and relative ease of implementation, is spindle speed variation (SSV), which consists in a continuous modulation of the nominal cutting speed. Sinusoidal spindle speed variation (SSSV) is a specific technique that exploits a sinusoidal law to modulate the cutting speed.
The vast scientific literature on SSV was mainly focused on cutting process stability issues fully neglecting the study of the mechanics of chip formation in SSV machining. The aim of this work is to fill this gap: thus, finite element method (FEM) models of Ti6Al4V turning were setup to simulate both SSSV and constant speed machining (CSM). The models consider both the micro-geometry of the insert and the coating. Numerical results were experimentally validated on dry turning tests of titanium tubes exploiting the experimental assessment of cutting forces, cutting temperatures and chip morphology. Tool-chip contact pressure, tool engagement mechanism and the thermal distribution in the insert are some of the analysed numerical outputs because they cannot be easily assessed by experimental procedures. These quantities were useful to compare thermo-mechanical loads of the insert both in CSM and SSSV machining: it was observed that the loads significantly differ. Compared to CSM, the modulation of the cutting speed involves a higher tool-chip contact pressure peak, a higher maximum temperature and higher temperature gradients that could foster the main tool wear mechanisms.

Keywords: titanium turning; spindle speed variation; finite element modelling

1 INTRODUCTION AND STATE OF THE ART

Titanium alloys are highly appreciated by the aerospace industry thanks to their great mechanical properties such as excellent resistance to weight ratio, high toughness and good corrosion resistance. On the other hand, titanium alloys are hard-to-machine mainly because of a low thermal conductivity that determines several drawbacks (chemical diffusion between tool surface and workpiece, quick delamination of insert coating on the flank, craterisation on the rake face). Because of their poor machinability, titanium alloys are generally processed with moderate cutting parameters. In rough turning, in order to avoid premature tool failure, cutting speed v_{C0} and feed rate f are never set respectively above 60 m/min and 0.4 mm/rev. Indeed, the only way to increase productivity is to increase depth of cut. Unfortunately, this increment exposes the process to a major risk of regenerative chatter.
Regenerative chatter is a specific cutting process instability that, involving very high tool-workpiece relative vibrations, can negatively influence almost all cutting operations [1], [2] and [3]. An instability analysis of machining process by a dynamic model of a turning machine is presented by Mahdavinejad [4]: the comparison between the natural frequency of the FE modeling and model testing showed the closeness of results. Severe vibrations may deteriorate the machined surface quality, facilitate tool wear and even damage some machine components. Indeed, chatter vibrations limit the achievable material removal rate and thus the machine productivity. Spindle speed and depth of cut are the process parameters that mainly affect the process stability. Spindle speed variation (SSV), first studied by Weck et al. [5], is a chatter suppression technique that, through a continuous and controlled modulation of spindle speed, can break the regenerative effect avoiding the growth of vibrations. In some scientific works it was observed that SSV technique seems more effective when low nominal cutting speeds, compared to the limiting machine dynamics, are required [6]. Albertelli et al. [7] showed that SSSV does not negatively influence the surface finish even if it is used for stable turning operations. Although SSV is certainly able to mitigate vibrations, its diffusion in the industrial shop floors is still limited (Siddhpura et al. [8]). In fact, the implementation of SSV requires an additional spindle torque and involves a higher energy consumption. The lack of a deep knowledge on the mechanics involved in the material removal process when the SSV is adopted still represents a major obstacle to a broad diffusion of the technique. In order to bridge part of the knowledge gap Albertelli et al. in [9] started studying the effect of spindle modulation on tool life: some steel turning tests revealed that spindle speed variation, applied in stable conditions, involves a tool life reduction. Tirelli and Chiappini [10] also performed some tool life tests on Ti6Al4V: a moderate tool life reduction was observed when SSSV was adopted instead of constant speed machining (CSM).

In this work, an FEM model of SSSV machining was adequately set and exploited in order to analyse thermal and mechanical consequences of the cutting speed modulation on the loads on the tool, on chip formation mechanisms and to provide some useful information to interpret the results of the aforementioned screening experimental studies [9], [10]. A detailed analysis of chip geometry at very high cutting speeds for Ti-6Al-4V alloy was performed by Sutter et al. [11]. The scientific literature about thermal and mechanical simulation of titanium alloys machining is quite rich; a lot of guidelines are available in order to select the physical and mechanical properties of both the workpiece and the tool, so that realistic results are made possible both for 2D and for 3D models (e.g. [12], [13]). Numerical simulation results mainly depend on the selected material model, the fracture criterion, the friction model and thermo-mechanical properties of both the tool and the workpiece, Filice et al. [14].
The most widely adopted material model in titanium alloys machining simulation is described by the Johnson - Cook law [15] which relates material flow stress to strain, strain rate and temperature. Different material-dependent parameters must be determined: Lee at al. [16] suggested a set of parameters that guarantees quite accurate results in titanium alloys machining simulation. Calamaz et al. [17] and Karpat et al. [18] improved the Johnson - Cook material model in order to simulate flow softening which generally occurs when certain values of strain and temperature are reached, however the results by Calamaz et al. showed a mismatch between experimental and predicted forces: the numerical results were lower than the experimentally measured forces. Chip segmentation can be reproduced both using fracture criterion (typically Cockroft and Latham [19]) or introducing material flow softening. Sima et al. [20] adopted the flow softening approach but numerical results showed that the predicted thrust force is considerably lower than the experimentally measured one. Calamaz et al. [17] compared experimental and numerical results obtained using a material behaviour that involves flow softening criteria. The comparison showed that the prediction error does not goes below 20%. Moreover, it was demonstrated that Cockroft and Latham allowed to get a better prediction of the chip morphology compared to flow softening approach.
Friction coefficient is one of the most influent parameters on the numerical results. Even if Ozel et al. [21] found that more realistic results can be reached using a variable friction model, many authors typically use a constant shear model [22] and [23]. Recommended values of the constant shear factor 'm' for Ti6Al4V cutting simulation vary from 0.4 to 0.7. The friction coefficient seems to have a heavy effect on thermal outputs but not on mechanical ones [16]. Burhanuddin et al. [24] found *m* equal to 0.6 to be the most appropriate value for thermal prediction.
Tool temperature cannot be easily calculated at the steady state because it is used, due to the high computational time, to simulate only a very short period of the machining process (in the order of milliseconds). Two approaches are therefore usable to force the achievement of steady state conditions: 1) to perform a thermal-only simulation for some seconds based on the total thermal energy that flows into the tool [25]; 2) to artificially increase the heat transfer coefficient at the tool-chip interface [18]. Thermal models, considering plastic deformation and tool-chip friction as the main heat sources, were proposed in literature by Cotterell et al. [26] and Adil et al. [27] in order to predict temperature both in the primary shear zone and the rake-chip zone.
In this work a 2D coupled thermo-mechanical FE model was developed with Deform2D™ and validated by experimental turning tests in dry orthogonal conditions of Ti6Al4V tubes. A thermocouple was positioned into the insert close to the rake face in order to measure the temperature in the cutting area. A dynamometric plate was used to measure experimental cutting forces. An optical microscope was used to analyse the chip morphology. Finally, a plain thermal model of the tool was built and fine-tuned to match the experimental results, in order to correctly predict the temperature distribution. The most important simulations results are the temperature and stress distributions along the tool-chip interface and how these quantities are related both to the instantaneous cutting speed and to the tool-workpiece engagement. These are useful information to deeply understand the phenomena involved in SSSV cutting and to model the evolution of process related quantities which are cannot directly evaluated experimentally.

2 FEM MODELS SETUP

In this Section it is shown how the FEM model was setup to reproduce both a CSM (constant speed machining) and an SSSV orthogonal Ti6Al4V turning process. The commercial software DEFORM-2D was adopted. The model validation is presented in Section 4. Numerical simulations were performed in two separated steps: 1) a thermo-mechanical simulation was done to predict cutting forces and temperature both in the workpiece and at the tool-chip interface; 2) a thermal only simulation was performed (just for SSSV case) to predict the temperature distribution inside the tool during cutting at the steady state conditions. Unlike conventional simulations of steady state machining, all state variables can never be considered constant over time, but they follow a periodic law. Thus, in this paper every time the expression 'steady state condition' is referred to an SSSV dependent variable, it means that the variable has reached its periodic steady-state condition. Fig. 1 shows the overall FE model and the location of the thermocouple head used during the real tests.

2.1 CSM and SSSV fully coupled thermo-mechanical simulations: description and objectives

Coupled thermo-mechanical simulations were performed to evaluate, in CSM and SSSV machining, the following variables: cutting forces, temperature and contact pressure along the tool-chip interface and the morphology of the chip. The SSSV simulation reproduced machining for two periods of the modulating law: i.e. one second when a 2 Hz speed variation law is adopted, which corresponds to a cutting length of 667 mm at the adopted cutting speed of 40 m/min. This is an extremely long time for FEM simulations, where generally just a few milliseconds of cutting process

are reproduced. To the authors' knowledge, such a long period of simulated time is unprecedented for FEM simulation of machining with implicit solvers. A code with implicit time integration scheme was chosen because it is inherently more accurate than explicit ones. Mesh windows allowed to generate a finer mesh at the tool-chip interface region with a mean element size equal to 0.025 mm and the remesh was performed by an auto-remeshing algorithm. The workpiece was modelled by using 3000 elements while the tool was modelled with 1000 elements. A very high computational time was accepted without sacrificing the mesh quality, depicted in Fig. 1 at the beginning of the FEM run. The simulation computational time was about 500 hours.

Workpiece length. The initial length of the material to be processed was 25 mm. A simulation of 1 second was possible by opportunely arranging, at discrete time intervals, both the portion of the workpiece not yet involved in the cutting and the already processed part. Since the workpiece fed the tool according to X-axis direction (Fig. 1), when the outer side (on the left) of the workpiece was 5mm far from the cutting edge the simulation was stopped and a the workpiece was restored: the already machined portion of work, passed the tool tip was trimmed and a new unprocessed piece of material was added ahead of the tool in order to regenerate a 25 mm total length. The state variables and the boundary conditions were updated by interpolating the final results of the previous run. Although this technique produced some limited errors due to extrapolation on the new portion of material, this errors became totally negligible after a few simulation steps.

Workpiece height. Also the workpiece height was chosen in order to reach a compromise between a realistic representation of the actual height and the computational time. A higher workpiece should guarantee a more accurate force prediction (reduced effects of the boundary conditions) but implies higher computational time. It must be observed that, since the remeshing algorithm works with a constant number of elements, higher workpiece also means a coarser mesh on the shear zone. Preliminary numerical simulations (considering different chip thickness/workpiece height ratios) of constant speed turning were performed in order to select a reasonable workpiece height, which was found to be 0.7 mm. For instance, if increasing the height up to 1.4 or 2.1 mm, very limited changes were registered on the cutting force and temperature profiles.

The FEM model was used to estimate different quantities and to analyse aspects that can be affected by the modulation of the cutting speed. Both numerical cutting forces and the morphology of the chip were compared to the experimental ones. The analysis of the obtained results is presented in the following paper sections.

The tool geometry was accurately modelled exploiting the micrograph (Fig. 1) of the cross-section of the adopted CNMG 120408 insert (with 3 μm of TiAlN coating). Moreover, considering the geometry of the adopted tool-holder (PCLNL 2525 M12), a 4.6° true rake angle γ_r was estimated. The main parameters adopted in the numerical simulations are summarized in Tab. 1.

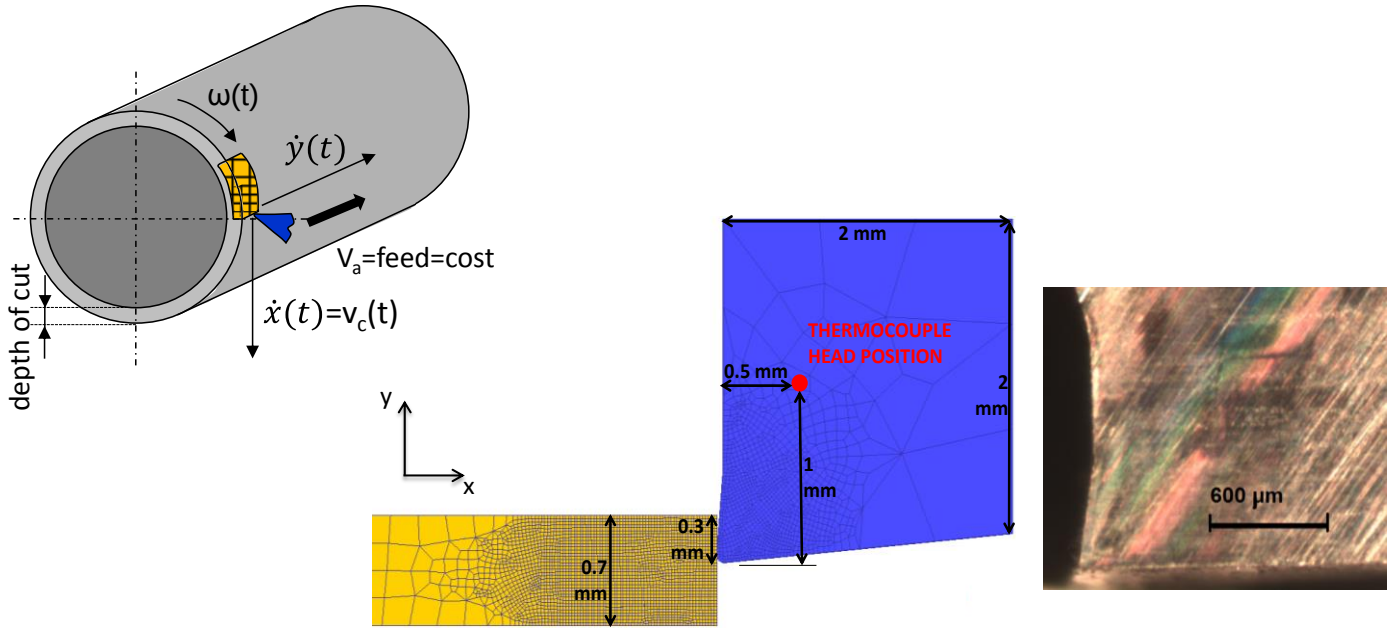

Fig. 1. Tool and Workpiece modelling and detail of tool micrograph

In order to allow a proper FEM modelling of SSSV cutting, a detailed analysis of the main cutting parameters (i.e. spindle speed, feed rate, depth of cut) when the sinusoidal modulating law is involved is imperative. Since the cutting speed is modulated through a sinusoidal law, the instantaneous chip thickness periodically varies. In order to be able to properly reproduce a SSSV cutting operation, a specific time-dependent trajectory has to be defined for the relative motion between the tool and the workpiece. The tool is ideally fixed to the ground, in order to facilitate the definition of the local remeshing window around the tool tip, and the workpiece translates. Two velocity boundary conditions were

set to the workpiece (Fig. 3): one along the X-axis (to model the cutting speed variation) and the other along the Y-axis (to reproduce the modulation of the chip thickness). During SSSV cutting the spindle speed follows Eq (1).

$$\omega(t) = \omega_0 + \omega_0 \cdot RVA \cdot sen(2 \cdot \pi \cdot fr \cdot t) \tag{1}$$

ω_0 is the nominal spindle speed, *fr* is the frequency of sinusoid and the ratio of variation amplitude (*RVA*) is a dimensionless parameter linked to the amplitude of the speed modulation:

$$RVA = \frac{\omega_{max} - \omega_0}{\omega_0} \tag{2}$$

where ω_{max} is the maximum spindle speed.

SSSV simulation		**CSM simulation**	
Mean v_{c0} [m/min]	40	**v_{c0} [m/min]**	40
Mean feed rate (*f*) [mm/rev]	0.3	**Feed rate (*f*) [mm/rev]**	0.3
SSSV *RVA*	0.3		
SSSV frequency (*fr*) [Hz]	2		

Tab. 1. First step simulation parameters both for CSM and SSSV

For CSM (Constant Speed Machining) the following relationship is valid:

$$v_a[mm/\min] = f[mm/rev] \cdot \frac{\omega \cdot 60}{2 \cdot \pi}[rev/\min] \Rightarrow f = \frac{v_a \cdot 2 \cdot \pi}{\omega \cdot 60} \tag{3}$$

where v_a is the lathe feed velocity, *f* is the feed rate (corresponding to the chip thickness). Introducing an acceptable approximation [28], the use of Eq. (3) can be also extended to SSSV cutting using a time-dependent *ω(t)* curve. As shown in Fig. 2, Eq. (4) and (5), the approximation comes from the need to avoid to solve the integral equation for the computation of τ that is the time required by the workpiece to perform a single revolution. If τ is approximated with t* the following equations can be written:

$$\tau(t) = \tau(\omega(t)) \cong t^* = \frac{2\pi}{\omega(t)} \tag{4}$$

$$f(t) \cong \frac{V_a}{60} \cdot t^* = \frac{V_a}{60} \cdot \frac{2\pi}{\omega(t)} \tag{5}$$

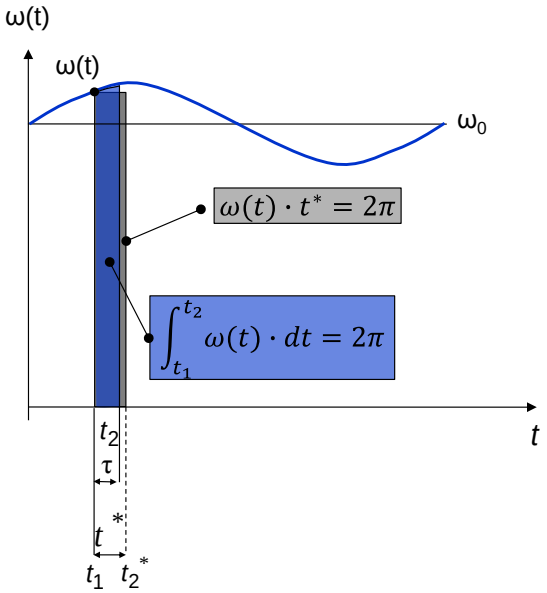

Fig. 2. Modulated spindle speed and delay approximation

It is important to observe that, in SSSV cutting, the lathe feed velocity v_a is kept constant: v_a can be computed considering the nominal spindle speed and the nominal feed rate.
Velocity boundary conditions along X was applied to the workpiece according to (6).

$$\frac{dx}{dt} = v_C(t) = \frac{d}{2} \cdot \omega(t) = \frac{d}{2} \cdot \left[\omega_0 + \omega_0 \cdot RVA \cdot sen(2 \cdot \pi \cdot fr \cdot t)\right] \quad (6)$$

Where d is the external diameter of the tubes used in the experimentation (d= 42 mm). Starting from Eq. (3) and Eq.(6), the Y axis workpiece speed law can be computed as follows:

$$\frac{dy}{dt} = \frac{\partial f}{\partial t} = -2\pi \cdot fr \cdot f \cdot \omega_0 \cdot \frac{[\omega_0 \cdot RVA \cdot \cos(2\pi \cdot fr \cdot t)]}{[\omega_0 + \omega_0 \cdot RVA \cdot sen(2\pi \cdot fr \cdot t)]^2} \quad (7)$$

The adopted SSSV is described by the following parameters: nominal cutting speed v_{C0}= 40 m/min, RVA = 0.3 and SSSV frequency fr=2 Hz. The nominal undeformed chip thickness 'f' was 0.3 mm/rev. The total simulated machining time was one second, corresponding to two periods of the modulating speed law.
The workpiece velocity boundary conditions set to perform the numerical simulations (v_c and df/dt) are shown in Fig. 3.
According with Umbrello [16] the Cockroft-Latham fracture criterion with a critical damage value of 245 MPa was adopted. A tabular definition of the Ti6Al4V flow stress model was adopted, as a function of strain, strain rate and temperature. The implemented friction law is based on the simple constant shear hypothesis $\tau = m \cdot \tau_0$, where m=0.7 is the constant friction factor and τ_0 the shear yield stress. The m value was updated considering experimental tests performed at constant speed. In the following paragraph the comparison between numerical and experimental cutting forces in SSSV regime will be presented. Flow stress and friction factor have been selected according to preliminary studies [29].
In order to effectively exploit the numerical simulation results, it was mandatory to simulate the process for one second (two periods of the speed law) to have at least one period data at the steady-state conditions, when the initial thermal transient phase has completely run out. It was also important to reach thermal steady state conditions on the rake face as fast as possible and for, at least, a whole period of the SSSV law, so a large artificial value of heat transfer coefficient h at the tool chip interface is required. Common values used in literature vary from 1000 to 100000 N/(mm*s*K), hence there is not a shared opinion about the more suitable value for this parameter [14], [20], [25]. Since a realistic h-value would be below 100 N/(mm*s*K), any choice between 1000 N/(mm*s*K) and 100000 N/(mm*s*K) represents a numerical "trick" anyway. A preliminary sensitivity analysis was performed in order to better understand the influence of this parameter on tool-workpiece interface regime temperatures and cutting forces. The simulations were performed at CSM. The steady-state results did not show strong differences between the three analyzed cases (h=1000 N/(mm*s*K), h=10000 N/(mm*s*K) and h=100000 N/(mm*s*K)) both for forces and temperatures prediction. As an example, if increasing h from 1000 to 10000 N/(mm*s*K), the temperatures on the tool surface increase less than 5%. Considering the performed analysis and the high involved computational time h=10000 N/(mm*s*K) seems to represent an acceptable compromise in order to limit the influence of the initial thermal transient.

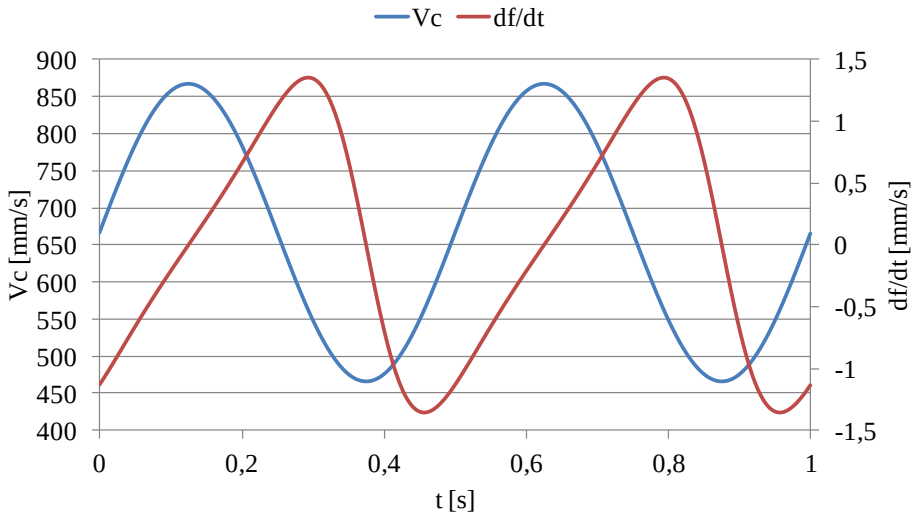

Fig. 3. Workpiece speed along X-axis (v_c) and Y-axis (df/dt)

2.2 Pure thermal simulation for SSSV: description and objectives

A total machining time of one second is long enough to predict “steady state” forces and temperatures at the tool-chip interface, but it is not sufficient to accurately evaluate the thermal load of the whole insert. This is useful to fully understand the thermo-mechanical behaviour of the insert. Thermal simulations are computationally much lighter than fully coupled thermo-mechanical simulations and much longer process times can be affordably simulated. A second-step thermal-only FEM model was therefore implemented, reproducing a machining period of 10 seconds (20 periods for 2 Hz SSV). The first-step thermo-mechanical model allows to get reasonably accurate thermal boundary conditions because of the high strain rates that can be observed close to the tool-work material interface. In this region the heat production rate is very high and the local thermal dynamics is very fast, not significantly affected by the initial thermal transient. This allows to use the thermo-mechanical model simulation results to feed the thermal simulation of the insert.

The most important parameter for the analysis of the thermal behaviour of the insert during a pure thermal simulation is the convection coefficient *c* which rules the heat transfer with the external environment. The thermal model was updated exploiting the experimental temperature measurements performed in the cutting tests. The *c*-value was calibrated to obtain temperature values, in the zone close to the thermocouple head, as close as possible to the experimental measurements. Only a portion of the real tool was modelled (dimensions are shown in Fig. 1), so the convection coefficient *c* had to be adapted in order to take into account both the considered geometry and the real convection conditions. The heat exchange conditions with the environment were set along the perimeter of the tool, not in contact with the workpiece.

3 EXPERIMENTAL TESTS

SSSV and CSM orthogonal cutting experiments were performed. The main objectives can be summarized as follows:

- validate the ‘first step’ thermo-mechanical simulations;
- measure the temperature in a zone close to the rake face (thermocouple location in Fig. 1), both to update the thermal model and to analyse the insert thermal load over the SSSV period and in CSM;
- compare cutting forces and chip morphology between constant and variable speed machining.

3.1 Experimental setup

All machining tests were performed using a CNC Somab Unimab 400 lathe with a maximum spindle speed of 2560 rev/min and a drive motor rated up to 11 kW. The lathe is equipped with a Numerical Control (NC) and with analogue drives. In order to be able to set the desired spindle speed law, the speed control loop was bypassed and the speed reference signal was generated directly from an external computer and sent to the spindle motor drive. An acquisition board (National Instruments ‘cDAQ 9174’) was used also to acquire forces, temperature, encoder signal and as an interface between the computer and the NC. The encoder data acquisition was used to experimentally compute the instantaneous chip thickness.

Cutting forces were acquired during the tests through a Kistler 9265 dynamometer that was interposed between the tool and the lathe turret. Titanium Ti6Al4V hollow cylinders (*d*=42 mm outer diameter and 1.6 mm wall thickness) were used in the experimental campaign in order to reproduce orthogonal cutting conditions. The adopted tool holder was a Sandvik ‘PCLNL 2525M’ and the carbide inserts were Sandvik CNMG 120408 SMR 1115 drilled by electro discharge machining (EDM) to obtain a hole with 0.8 mm diameter and 4.1 mm depth, this allows the ‘K’ thermocouple head to be positioned as close as 0.5 mm away from the rake face.

3.2 Experimental results

Orthogonal dry cutting tests with the following parameters were performed: nominal cutting speed v_c= 40 m/min, spindle speed modulating frequency 2 Hz, *RVA*=0.3, nominal feed rate equal to 0.3 mm/rev. To identify and analyse the thermal transient, experimental data were measured and acquired for at least 25 seconds. During the cutting trials, forces, temperature and data from the spindle encoder were acquired. Seven replicates both for constant and variable speed conditions were performed. In Tab. 2 the mean and standard deviation values for the main harmonic components of the main cutting force *Fc* and thrust force *Ff* are reported, calculated by averaging the seven replicates. In order to facilitate the comparison to the FEM results, the force values were referred to the depth of cut unit, i.e. they were divided by 1.6 mm, which is the tube thickness.

	SSSV				***CSM***			
	Fc			*Ff*	*Fc*			*Ff*
	0 Hz	2 Hz	5.8 Hz	0 Hz	0 Hz	2 Hz	5.8 Hz	0 Hz
Mean [N/mm]	517	99	-	232	494	-	13.5	219
Std. Dev. [N/mm]	12.9	11.8	-	12.4	18.2	-	4.3	10.5

Tab. 2. Experimental results, mean and standard deviation values out of 7 replicated tests

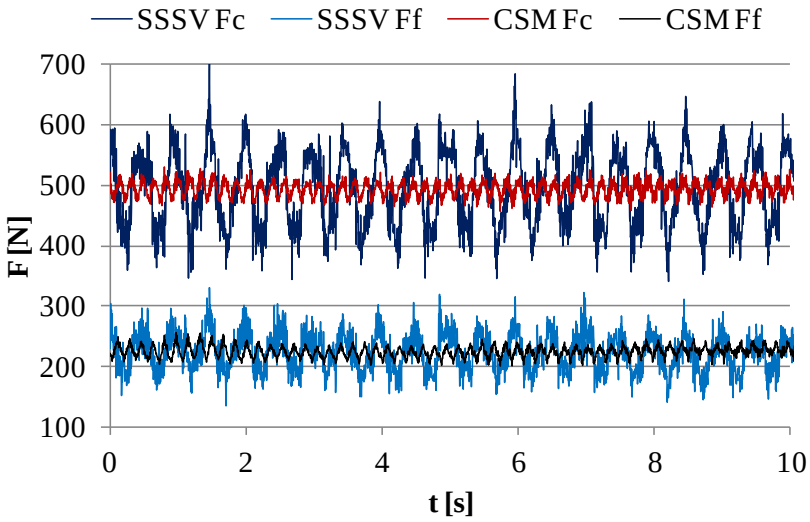

Fig. 4. Example of experimental cutting forces and feed (thrust) forces (for unit of depth of cut).

Tab. 2 also reports the synthetic results of fast Fourier transforms (FFTs) performed on each force acquisition. Considering SSSV signals the main frequency observed is, as expected, 2 Hz. For CSM signals the main frequency present is equivalent to about 5.8 Hz and is due to the rotation of the tube (348 rpm). Components of the force signals at larger frequencies, i.e. correlated to the chip segmentation frequency, cannot be caught with the available experimental setup. Fig. 4 shows an example of the measured experimental cutting and thrust forces.
In statistical terms, the mean force values for both SSSV and CSM are equal. As a proof, a 2-sample t-test was performed considering I-type error threshold α=0.05 and the following p-values were obtained: 0.086>0.05 for *Fc* and 0.426>0.05 for *Ff*.
While the Constant Speed Machining allows to reach a constant steady state temperature in the thermocouple zone, the variable speed of SSSV process causes a time dependent temperature wave. As a reference for the thermal-only model, experimental temperature measurements were performed by positioning a thermocouple head inside the tool, at about 0.5 mm away from the tool rake face. It was observed that about 15 seconds after the starting of the test the thermal transient can be considered finished. After this transient, an average temperature equal to 625°C was measured. In Fig. 5 both the temperature measurement and the associated cutting speed were reported. As it could be expected, a temporal delay (0.125 s) between speed and temperature can be appreciated, obviously due to the time required for heat propagation.

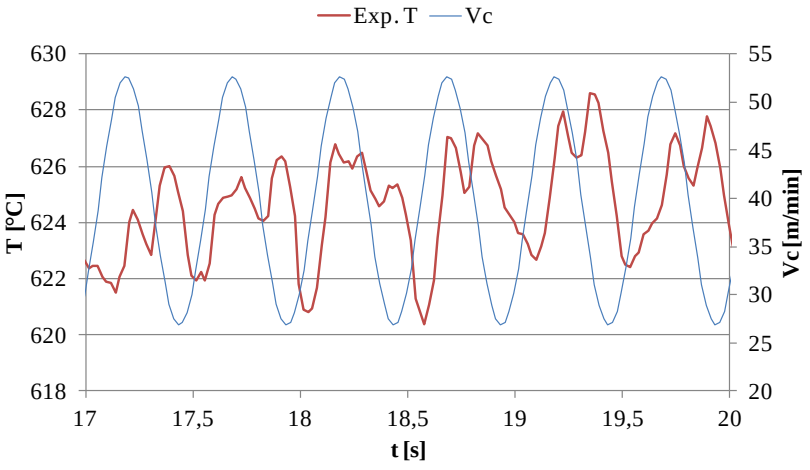

Fig. 5. SSSV: experimental temperature vs. cutting speed

4 THERMO-MECHANICAL FEM MODELS RESULTS AND ANALYSIS

4.1 Comparison with experimental results

In 2D simulations, that well reproduce orthogonal cutting conditions, there is no radial force and numerical outputs consist in just two forces (calculated for unit of depth of cut 'b'): *fx* (representing the cutting force F_c) and *fy*

(representing the thrust force F_f). Forces reach steady state in a very short time but, in order to avoid thermal transient effects, force results were considered for the second period of SSSV machining simulation (from 0.5 to 1 second). Simulated force signals may exhibit the dependency on the SSSV modulation and on the chip segmentation phenomenon. The segmentation frequency is predicted by FEM as oscillating between 1200 Hz and 3900 Hz. The simulated SSSV cutting and thrust forces also show a 2 Hz periodic path which correctly follows the feed rate variation law. The amplitude at this frequency for the main cutting force was predicted by FEM with an error over experiments of about 16%, as reported in Tab. 3. The average value of main cutting force *Fc* was very well predicted by FEM. Thrust force *Fc* was underestimated, probably because the elastic springback of the workpiece material was not considered in the model.

	SSSV			CSM	
	Average F_c [N/mm]	Average F_f [N/mm]	*Fc* 2 Hz component amplitude [N/mm]	Average F_c [N/mm]	Average F_f [N/mm]
FE model	495	192	115	500	164
% difference with experimental values	-4.3%	-20.8%	+16.2%	+1.2%	-25%

Tab. 3. Simulated forces per unit depth and percentage difference with experimental values (**Tab. 2**)

In CSM simulations, the segmentation frequency was predicted at a value of about 1310 Hz. The experimentally measured 5.8 Hz main frequency cannot be numerically predicted, as there is no effects due to rotation (i.e. unbalance) in FEM. As a consequence, a comparison between FEM and experiments can only be performed in terms of average values, as shown in the right portion of Tab. 3.
As an example, a sample portion of the experimental force profiles is compared in Fig. 6 and Fig. 7 to the corresponding FEM profiles. In these figures, the simulated force signals were low-pass filtered at 125 Hz, which is the bandwidth of the experimental setup.

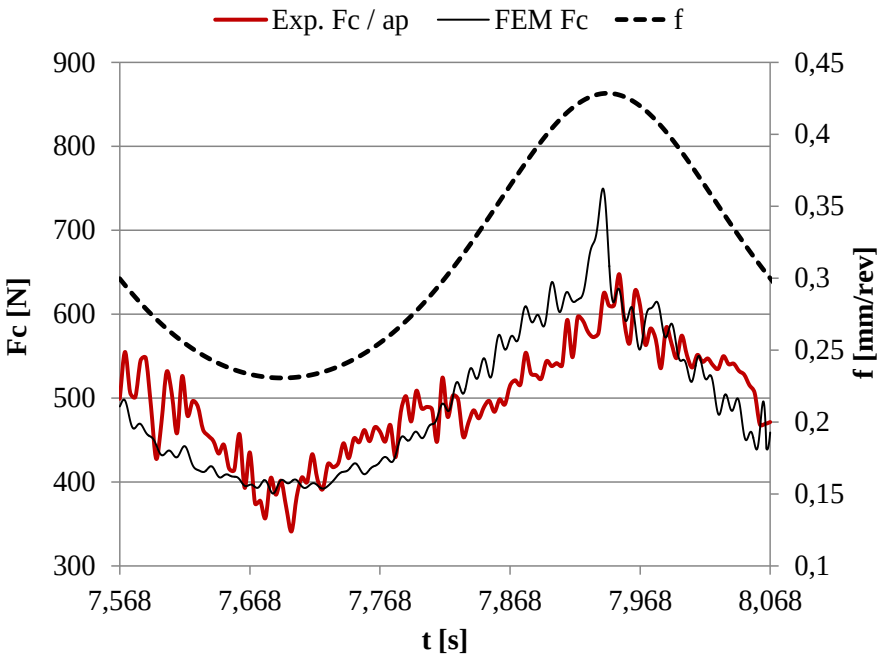

Fig. 6. FEM vs. experimental *Fc* (for unit of depth of cut) vs. feed rate law

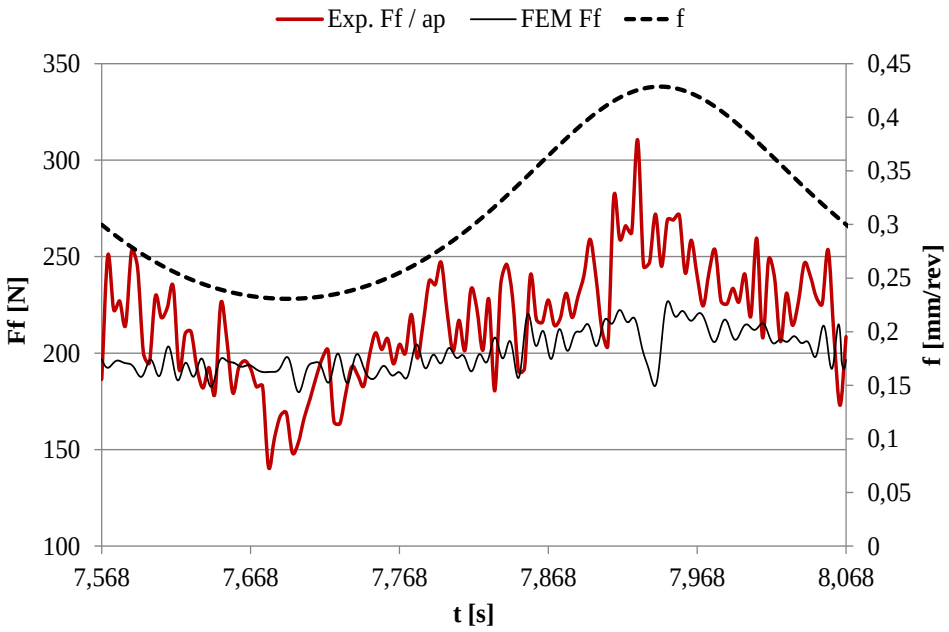

Fig. 7. FEM vs. experimental *Ff* (for unit of depth of cut) vs. feed rate law

Simulations were validated also in terms of chip morphology: the average chip thickness was obtained as the mean between peaks and valleys in several samples, collected during the tests and measured at the microscope. Considering CSM, chip thickness is influenced by the chip segmentation phenomenon and the FEM model nearly perfectly reproduces the experimental average chip thickness of 0.30 mm. An example of the serrated chip obtained by the FE model is reported in Fig. 8.

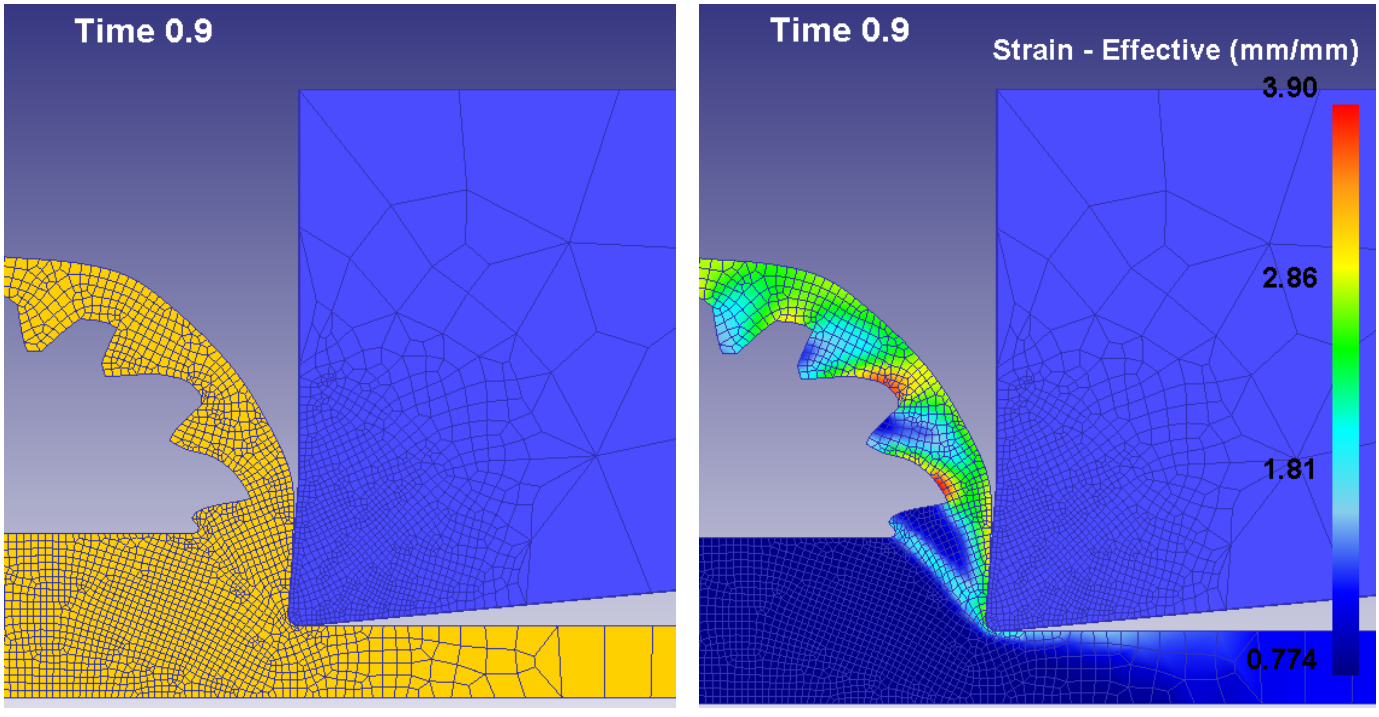

Fig. 8. Simulated serrated chip at 0.9 s: geometry (left) and strain (right)

For SSSV tests, 20 short chip samples were taken in a sequence and measured out of one period of machining (a time of 0.5 seconds). Thus it was possible to clearly observe how the average chip thickness ($\overline{f_{sample}}$) varies during the SSSV period. In Fig. 9 experimental mean chip thickness and the average peak to peak distance ($\overline{pp_{sample}}$) are depicted. Pi and Vi are respectively the peak height and the valley height.

$$\overline{f_{sample}} = 1/3 \sum_{i=-1}^{1} \left(\frac{P_i + V_i}{2} \right) \tag{8}$$

$$\overline{pp_{sample}} = 1/3 \sum_{j=-1}^{1} pp_i \tag{9}$$

Data reported in Fig. 8 refer to one of the 20 analysed specimens. Interestingly, both parameters of chip morphology follow a similar and clear trend, influenced by the speed law (i.e. the chip thickness modulation).
In SSSV machining simulation too the chip morphology is well reproduced, with similar minimum and maximum values of mean chip thickness and peak-to-peak distance. In Tab. 4 this morphology comparison is summarised.

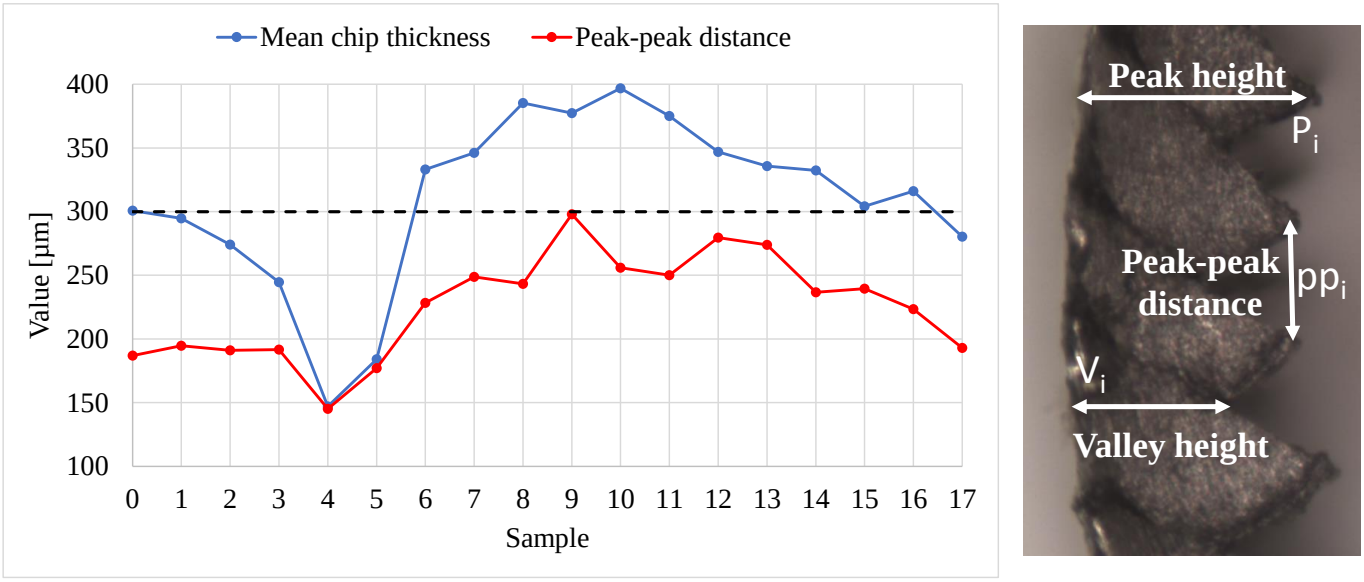

Fig. 9. Chip morphology: experimental measurements (average chip thickness and peak-peak distance)

	Average chip thickness [mm]		Valley height [mm]		Peak height [mm]		Peak-Peak distance [mm]	
	Max	Min	Max	Min	Max	Min	Max	Min
FEM	0.386	0.170	0.279	0.112	0.492	0.218	0.368	0.176
Experimental	0.397	0.147	0.300	0.102	0.496	0.193	0.298	0.145

Tab. 4. FEM and experimental chip morphology

4.2 Tool Thermal load analysis

Fully coupled thermo-mechanical simulations allow to estimate the temperature distribution and the contact pressure in each node along the rake face zone at steady state conditions. These results are very useful to analyse the complex tool engagement when SSSV is implemented and they can also be used to locate the most stressed tool zone. In Fig. 11, for instance, temperatures evaluated at points 5 and 16 (position indicated in Fig. 10) for the SSSV simulation are reported. It can be observed that point 16 was always engaged with the workpiece while point 5 was not always in contact with the forming chip: this is due to the modulation of the chip thickness as a result of the variation of the cutting speed (see Fig. 12). As the chip thickness increases, the tool-chip contact length increases as well, hence the considered points (5 and 16), suffer a similar thermal load (the two temperatures are almost identical at about 750 °C). On the other hand, when the chip thickness is low, contact length decreases, the thermal gradient gets higher and so the temperature difference of the monitored points. The tool-workpiece engagement heavily affects the tool thermal load and the tool-chip contact pressure. The mean temperature values for point 5 and 16 are 638°C and 838°C respectively.

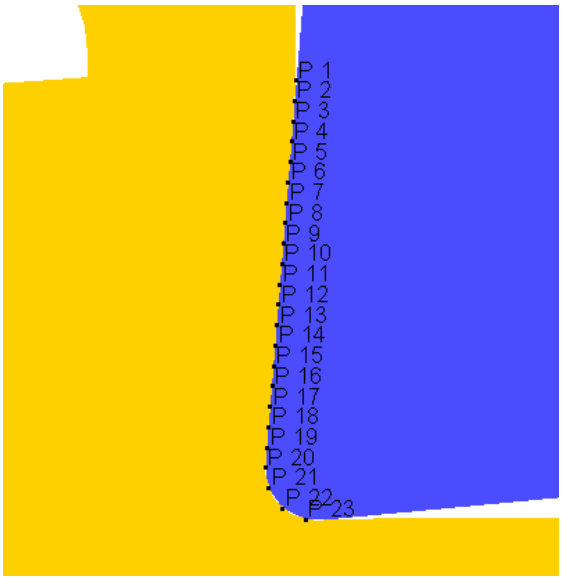

Fig. 10. Tool-chip interface points

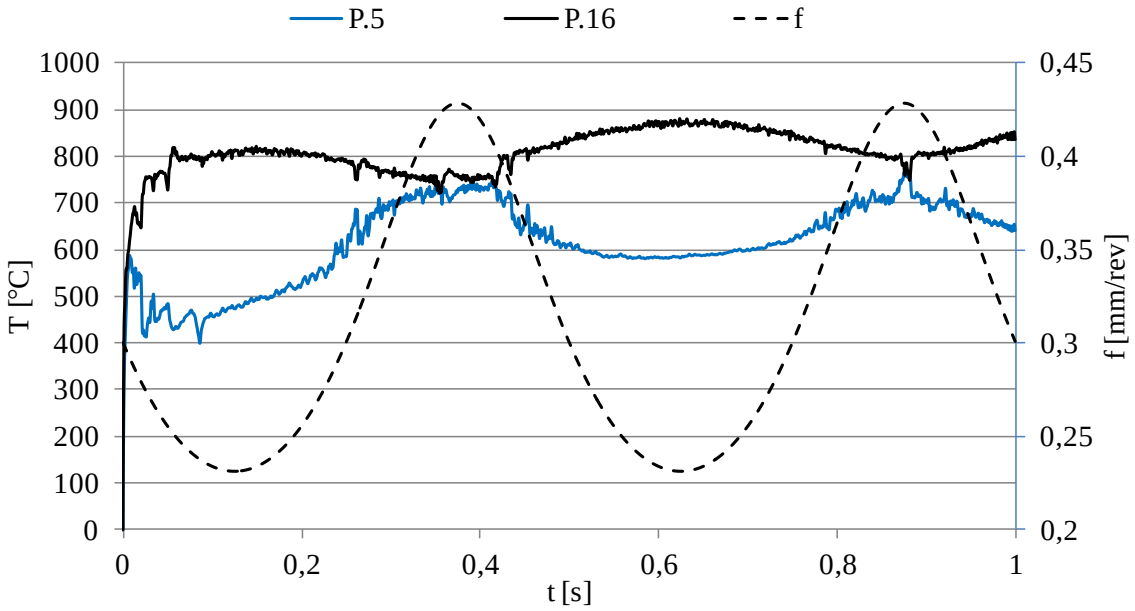

Fig. 11. Point 5 and point 16 thermal loads for SSSV simulation

For conventional machining, the temperature of rake face point does not follow a similar law because the chip thickness is constant and so the contact length (slightly influenced only by chip segmentation). The mean temperature values for point 5 and 16 are constant and equal to 659°C and 800°C respectively.

4.3 SSSV cutting mechanisms analysis and comparison with CSM

Thanks to the simulation results, an analysis of cutting mechanisms with SSSV is now possible. This section will show how, unlike CSM, SSSV machining determines variable pressure and temperature values on the tool-workpiece interface. Besides, maximum pressure and temperature values are not always registered at the same location (as in CSM), but they move along the tool rake surface. These variations might have either positive (due to temporary local stress release) or negative (due to fatigue) consequences on the surface integrity of the tool. They will be shown in detail and compared to the stationary conditions registered in CSM.
The tool-workpiece contact length and the deformed chip thickness were measured 17 times during one SSSV period and they are plotted respectively in Fig. 7 and Fig. 12.

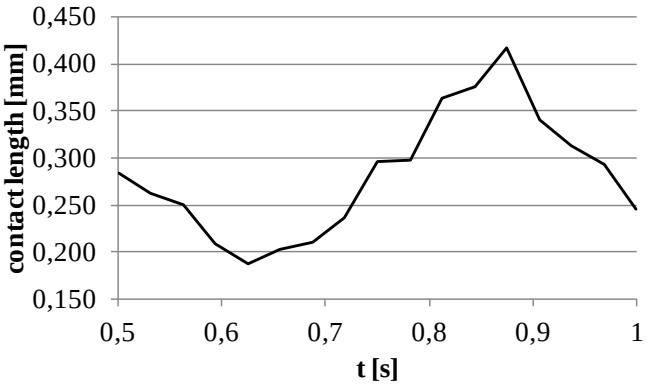

Fig. 12. Tool-chip contact length

In order to analyse the effect of a time-dependent tool-workpiece engagement an auxiliary reference system, in which "s" is a curvilinear coordinate along the tool cross-section profile, was adopted (Fig. 13). Over the SSSV period, the highest temperatures and contact pressures locations can be expressed through this curvilinear coordinate. As shown in Fig. 13, the position corresponding to the highest temperature moves along the tool rake. The maximum temperature is always located on the tool rake; lower temperatures are observed on the cutting edge radius and on the tool flank. The maximum temperature (865°C) can be observed at position 'A' (s=0.24 mm) when the cutting speed reaches the maximum value. On the other hand, when the chip thickness increases due to the speed decrement, the highest temperature value decreases and moves further away from the cutting edge (at point 'B', s=0.37 mm). The difference between minimum and maximum temperatures reached on the tool rake is about 100 °C. As already done for the temperature, in Fig. 14 the location of the highest contact pressure and its values are shown. During SSSV cutting, the highest contact pressure is always located close to the cutting edge (0.095<s<0.143 mm) and the maximum value (about 6005 MPa) over one SSSV period is reached at point 'C' (s=0.102 mm).

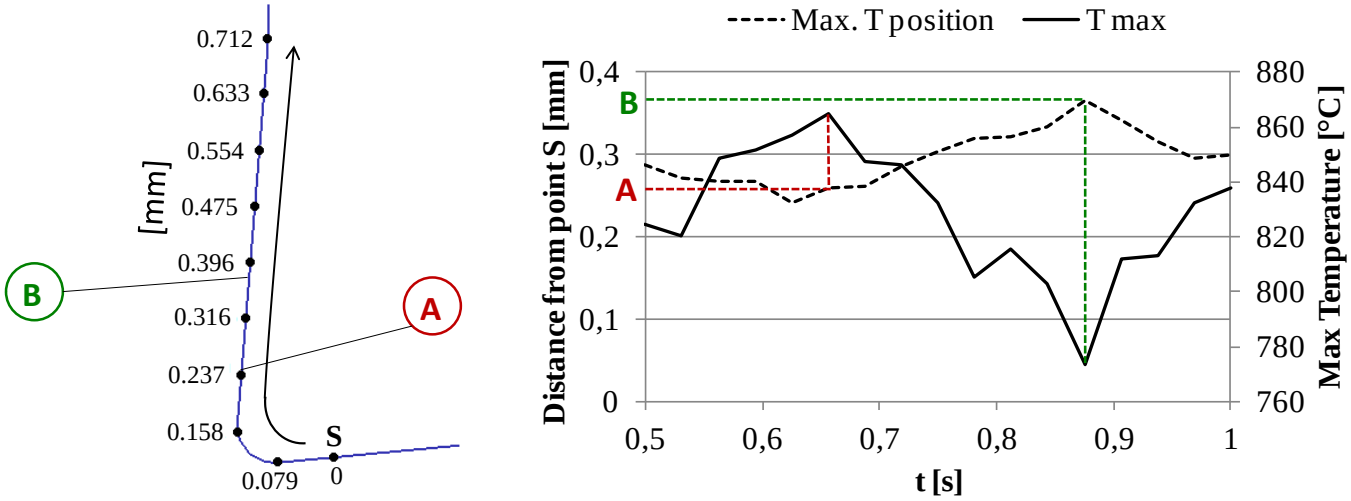

Fig. 13. Position of the highest temperature point and the linked temperature values

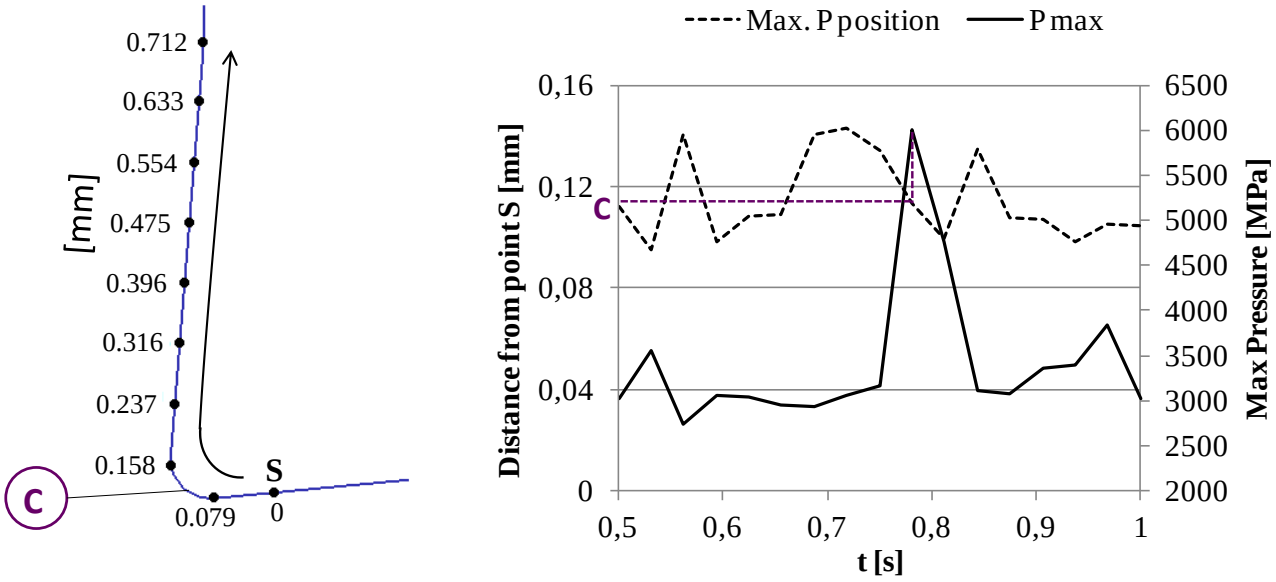

Fig. 14. Position and value of the highest pressure point along tool edge vs. time

The graph on the right of Fig. 15 clearly shows that the peak of pressure has to be associated to the peak of df/dt, i.e. the chip thickness variation velocity. The maximum value of pressure almost doubles when the maximum df/dt is reached. The location of the highest contact pressure point oscillates along the curvilinear coordinate, but this displacement is short, if compared to the displacement of the highest temperature location. With respect to the tool life, the cyclic variation of temperature and pressure values could be detrimental, as they induce an additional fatigue stress. Conversely, the movement of the points of maximum temperature and pressure could be considered as a positive effect, because the thermal and mechanical loads are distributed over a bigger surface.
Because of the substantially unvaried chip thickness, Constant Speed Machining does not present a periodic variation of pressure and temperature similar to SSSV, hence no mechanical or thermal fatigue stress is expected on the cutting edge and on the rake face. The maximum temperature point does not move and there are no time-dependent pressure peaks on the cutting edge. Referring to the reference system of Fig. 13 and Fig. 14 the maximum temperature point is located at 0.256 mm from 'S' and the corresponding value is about 826°C, the maximum pressure point is located at 0.095 mm from 'S' with a value of 5237 MPa. Hence CSM present a lower absolute maximum temperature (-4.5%) and pressure (-12.7%) but constant and fixed in space respect to SSSV.

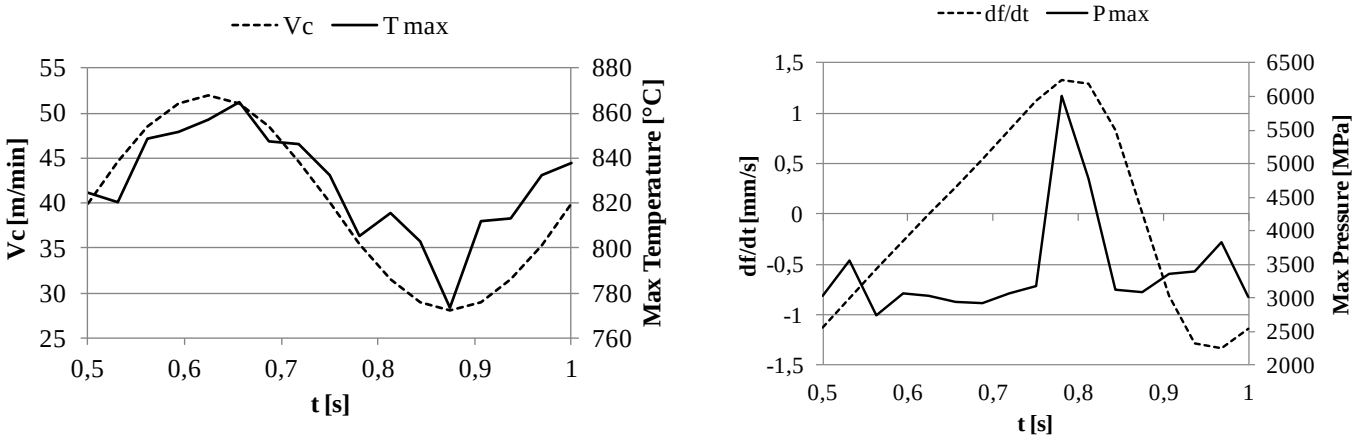

Fig. 15. Highest temperature as a function of v_c (left), highest contact pressure as a function of df/dt (right) variation

5 PURE THERMAL SIMULATIONS RESULTS

As previously described, a step-two thermal-only FE simulations was performed (starting from step 1 FEM results) for the SSSV case. The main goal of step-two simulations was to get a reliable thermal model of a bigger portion of tool,

avoiding the overwhelming computational issues involved in the thermo-mechanical coupled simulation. This model can be used to evaluate the tool thermal load both over a longer period of time and considering a bigger portion of tool. The FE model was updated exploiting the experimental data from the thermocouple (Fig. 5) and comparing it to the FE temperature at point P1. Convection coefficient *c* was fine-tuned, after preliminary sensitivity tests, starting from the value of 0.9 N/(s*mm*K). The best results were obtained for *c*=0.7 N/(s*mm*K) which guarantees a perfect agreement with the experimental measurement. In experiments, the insert exchanged heat with both environment and tool-holder surfaces. This cannot be reproduced in simulation, because a very small part of the insert is modelled. Thus in FE model the convection coefficient efficiency in prediction of tool internal temperature is strictly linked with tool material and tool geometry of each simulated case. It is more a numerical parameter than a physical property, indeed. However the adopted experimental configuration and the used tool geometry and coating are quite common in titanium rough turning. Hence the tuned FEM model results maintain a general validity, exploitable by future scientific works.

T [°C] at P1	
Max.	628
Min.	622

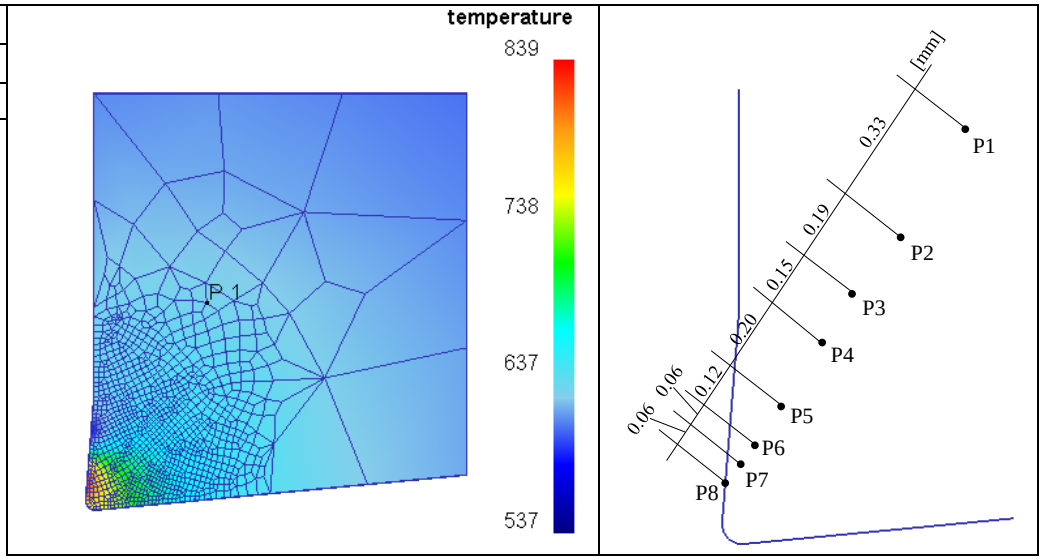

Tab. 5. FE temperature at P1; temperature map and location of points P1:P8

Once the thermal model had been validated, it was possible to analyse the thermal behaviour of some internal points of the tool, for instance starting from P1, the position of the thermocouple, towards the tool-chip contact zone (P8). Results are shown in Fig. 16.

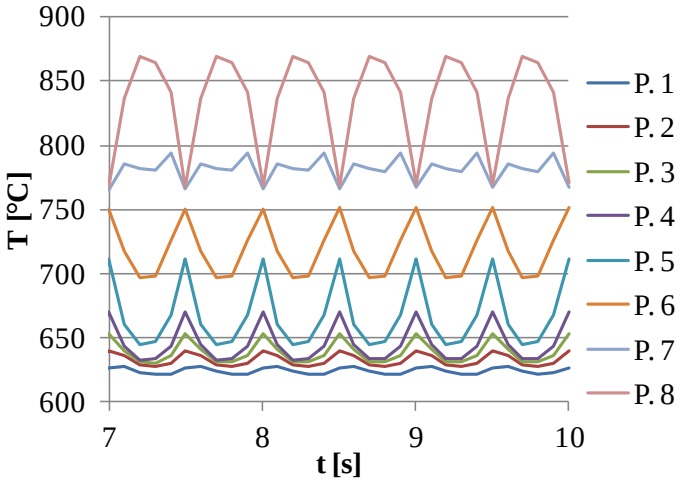

Fig. 16. Temperature vs. time for points P1:P8, plotted after a transient, i.e. when oscillations have become stable

Point 8 is placed on the rake face: its temperature variations are large with a profile similar to the *df/dt* law. Point 7 is only 0.06 mm away from P8, but its temperature variations are significantly damped.
Point 1 is relatively far from the surface, and its temperature is nearly flat; interestingly, P1 is hottest when P8 and P7 are down to their minimum temperature and vice versa. As the probe moves along the indicated line from P2 to P6, the temperature variations within one SSSV cycle increase up to about 50 °C. The thermal map of the insert in different instants of the SSSV period (0.5 seconds) was obtained and shown in Tab. 6.

Time instant		Time instant	
9.5 sec	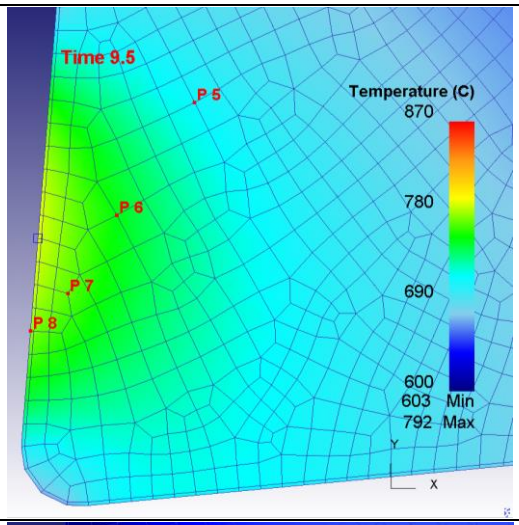	9.8 sec	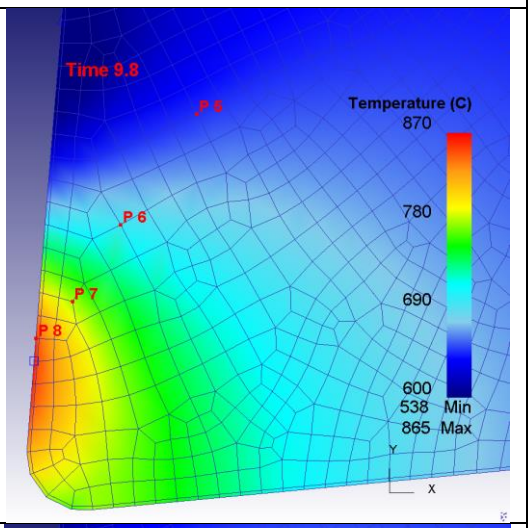
9.6 sec	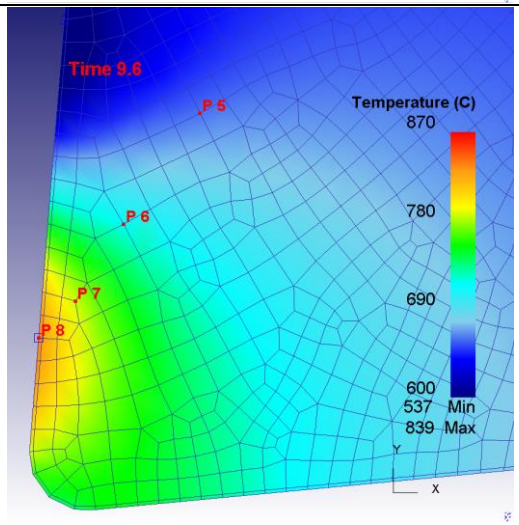	9.9 sec	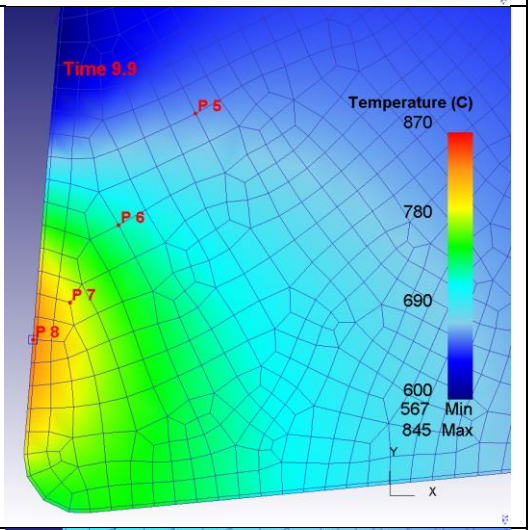
9.7 sec	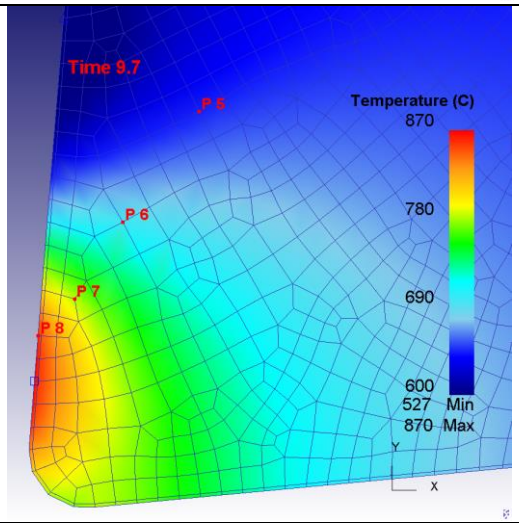	10 sec	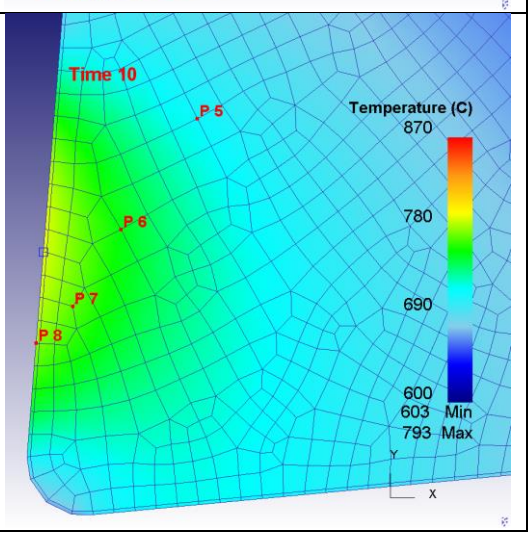

Tab. 6. Temperature evolution at steady state conditions inside the tool during an SSSV period

6 CONCLUSIONS

This work is part of a research line aimed at evaluating the Sinusoidal Spindle Speed Variation (SSSV) effects both on tool wear and integrity in view of a massive future industrial application. It is based on numerical simulations performed by means of an experimentally validated finite element model of the cutting process, which helps clarifying many issues involved in the application of Sinusoidal Spindle Speed Variation as a chatter suppression technique, in comparison to traditional constant speed machining processes. Most of the investigated variables are difficult or impossible to be observed experimentally.

Thermo-mechanic models of orthogonal sinusoidal spindle speed variation cutting and constant speed machining cutting were set. The thermo-mechanical models were validated by means of comparison to experimental measurements of cutting forces and chip morphology in dry turning tests of titanium tubes. The model accuracy was proved by a numerical-experimental cutting forces deviation of about 4% (for spindle speed variation) and 1.2% (for constant speed machining) with a realistic reproduction of serrated chip morphology even for variable speed cutting. For the variable speed case a thermal only simulation was setup and updated, thanks to a comparison with experimental temperature measurements, to predict the whole insert thermal load. This second stage simulation was performed imposing the time-dependent thermal boundary conditions obtained from the first thermo-mechanical simulation stage. Lastly the model was used to describe the thermal behaviour in a region between thermocouple location and rake face, getting a thermal map inside the tool.
The simulations results were deeply analysed and discussed. For Spindle Speed Variation machining it was found that the tool-workpiece engagement varies according to the chip thickness modulation. This affects the heat production (due to material deformation) and how the heat flows both in the tool and in the workpiece. When the chip thickness reaches the highest value (minimum cutting speed) heat is diffused along a higher tool-workpiece contact length while when the cutting speed reaches the highest value the heat flows through a limited contact region. Similar analyses have also been performed considering the tool-material contact pressure: it was observed that the maximum pressure can be always observed in a small region close to the cutting edge and the highest peaks of pressure are reached when df/dt (Y-axis speed in simulation) is maximum. The contact pressure exhibits a relevant oscillation during SSSV period. It was also observed that the highest thermal load and the highest contact pressure do not occur at the same time and in the same tool-material contact region. Unlike the traditional Constant Speed Machining, if a variable speed law is adopted, a thermo-mechanical cycle appears that might fatigue the tool. Furthermore, highest peaks of pressure and temperatures are reached in SSV compared to CSM. Thus, using a variable cutting speed in stable conditions, could decrease tool life.

REFERENCES

[1] M. Kayhan, E. Budak, An experimental investigation of chatter effects on tool life, Proc. Inst. Mech. Eng., Part B: J. Eng. Manuf., 223 (2009) 1455-1463.
[2] J. Tlusty, M. Polacek, The stability of machine tools against self excited vibrations in machining, Proc. Int. Res. Prod. Eng. Conf., (1963) 465-474.
[3] S.A. Tobias, W. Fishwick, The chatter of lathe tools under orthogonal cutting conditions, Trans. ASME, 80 (1958) 1079-1088.
[4] R. Mahdavinejad, Finite element analysis of machine and workpiece instability in turning, Int. J. Mach. Tools Manuf, 45 (2005) 753-760.
[5] M. Weck, E. Verhaag, M. Gather, Adaptive control for face-milling operations with strategies for avoiding chatter vibrations and for automatic cut distribution, Ann. CIRP, 24 (1975) 405-409.
[6] G. Quintana, J. Ciurana, Chatter in machining processes: A review, Int. J. Mach. Tools Manuf, 51 (2011) 363-376.
[7] P. Albertelli, S. Musletti, M. Leonesio, G. Bianchi, M. Monno, Spindle speed variation in turning: technological effectiveness and applicability to real industrial cases, Int. J. Adv. Manuf. Technol., 62 (2012) 59-67.
[8] M. Siddhpura, R. Paurobally, A review of chatter vibration research in turning, Int. J. Mach. Tools Manuf, 61 (2012) 27-47.
[9] P. Albertelli, V. Mussi, C. Ravasio, M. Monno, An Experimental Investigation of the Effects of Spindle Speed Variation on Tool Wear in Turning, Procedia CIRP, 4 (2012) 29-34.
[10] E. Chiappini, S. Tirelli, Tornitura del titanio aeronautico: simulazione e sperimentazione, in: Master's Degree Thesis, Politecnico di Milano, Corso di Laurea in Ingegneria Meccanica, 2012.
[11] G. Sutter, G. List, Very high speed cutting of Ti–6Al–4V titanium alloy – change in morphology and mechanism of chip formation, Int. J. Mach. Tools Manuf, 66 (2013) 37-43.
[12] G.M. Pittalà, M. Monno, Flow stress determination in orthogonal cutting process combining the primary and the secondary shear zones, Int. J. Mater. Form., 3 (2010) 483-486.
[13] G.M. Pittalà, M. Monno, 3D finite element modeling of face milling of continuous chip material, Int. J. Adv. Manuf. Technol., 47 (2010) 543-555.
[14] L. Filice, F. Micari, S. Rizzuti, D. Umbrello, A critical analysis on the friction modelling in orthogonal machining, Int. J. Mach. Tools Manuf, 47 (2007) 709-714.
[15] G.R. Johnson, W.H. Cook, A constitutive model and data for metals subjected to large strains, high strain rates and high temperatures, Proc. 7th Int. Symp. Ballist., (1983) 541-547.

[16] D. Umbrello, Finite element simulation of conventional and high speed machining of Ti6Al4V alloy, J. Mater. Process. Technol., 196 (2008) 79-87.
[17] M. Calamaz, D. Coupard, F. Girot, A new material model for 2D numerical simulation of serrated chip formation when machining titanium alloy Ti–6Al–4V, Int. J. Mach. Tools Manuf, 48 (2008) 275-288.
[18] Y. Karpat, Temperature dependent flow softening of titanium alloy Ti6Al4V: An investigation using finite element simulation of machining, J. Mater. Process. Technol., 211 (2011) 737-749.
[19] M.G. Cockroft, D.J. Latham, Ductility and workability of metals, J. Inst. Met., 96 (1968).
[20] M. Sima, T. Özel, Modified material constitutive models for serrated chip formation simulations and experimental validation in machining of titanium alloy Ti–6Al–4V, Int. J. Mach. Tools Manuf, 50 (2010) 943-960.
[21] T. Özel, The influence of friction models on finite element simulations of machining, Int. J. Mach. Tools Manuf, 46 (2006) 518-530.
[22] R. Alvarez, R. Domingo, M.A. Sebastián, Comparison of predicted forces in 2D and 3D FEM orthogonal cutting simulations of UNS A92024 and Ti6Al4V alloys, 12th CIRP Conf. Model. Mach. Oper., 1 (2009) 83-90.
[23] Y. Karpat, Finite element modeling of machining titanium alloy Ti-6Al-4V using a modified material model, 12th CIRP Conf. Model. Mach. Oper., 1 (2009) 107-114.
[24] Y. Burhanuddin, C.H.C. Haron, J.A. Ghani, Effects of edge geometry on the performance of CBN tools when cutting titanium 6Al-4V : experimental and simulation, 12th CIRP Conf. Model. Mach. Oper., 1 (2009) 211-217.
[25] D. Umbrello, L. Filice, S. Rizzuti, F. Micari, L. Settineri, On the effectiveness of Finite Element simulation of orthogonal cutting with particular reference to temperature prediction, J. Mater. Process. Technol., 189 (2007) 284-291.
[26] M. Cotterell, G. Byrne, Characterisation of chip formation during orthogonal cutting of titanium alloy Ti–6Al–4V, CIRP J. Manuf. Sci. Technol., 1 (2008) 81-85.
[27] G.K. Adil, V.K. Jain, T. Sundararajan, A finite element analysis of temperature in accelerated cutting, Int. J. Mach. Tools Manuf, 28 (1988) 577-590.
[28] L. Xinhua, B. Balachandran, Stability of Up-milling and Down-milling Operations with Variable Spindle Speed, J. Vib. Control, 16 (2010) 1151-1168.
[29] E. Chiappini, S. Tirelli, P. Albertelli, M. Strano, M. Monno, FEM simulation of Ti6Al4V turning with SSSV, AITeM Conf. Proc., S. Benedetto del Tronto (Italy), (2013).